Agricultural Water Management 213 (2019) 309–323

Contents lists available at ScienceDirect

Agricultural Water Management

journal homepage: www.elsevier.com/locate/agwat

A conceptual agricultural water productivity model considering under field capacity soil water redistribution applicable for arid and semi-arid areas with deep groundwater

Shilei Chen[a,b], Zailin Huo[a,*], Xu Xu[a], Guanhua Huang[a]

[a] Center for Agricultural Water Research in China, China Agricultural University, Beijing, 100083, PR China
[b] School of Water Resources and Hydropower Engineering, Wuhan University, Wuhan, 430072, PR China

ARTICLE INFO

Keywords:
Agricultural water productivity
The under field-capacity redistribution
Conceptual soil hydrological model
Deep groundwater
Arid and semi-arid areas

ABSTRACT

Agricultural water productivity (AWP) model is an essential tool for irrigation water management that is highly dependent on soil water processes. Soil hydrological models based on numeric solution to the Richards' equation are time-consuming and difficult to measure, and models based on soil water balance approach are favored especially for crop water simulation because of the less parameters requirement and higher operational efficiency. In most of the soil water balance models such as Williams-Ritchie water balance model, AquaCrop model and Hydrobal model, the under field-capacity redistribution (the redistribution during the period of soil water content below the field-capacity) is omitted and this treatment does not adequately simulate AWP for arid and semi-arid areas with deep groundwater. In these areas, AWP is the ratio between crop yield achieved and the sum of actual evapotranspiration and deep percolation at field scale. Since no more water supply for crop growth except for low frequency irrigation and tiny amount of precipitation, high evapotranspiration will aggravate an upward flow that can enhance transpiration and thus benefit crop growth while deep percolation not available for crop is sustainably accumulated to a considerable volume in under field-capacity redistribution process. To take into consideration the beneficial effects of upward flow on crop growth and the considerable under field-capacity deep percolation loss, a conceptual soil hydrological model considering under field-capacity redistribution (CSHMUR) is developed and coupled with the EPIC crop growth model. In CSHMUR model, soil water redistribution is characterized by two sequential water flows: downward flows affected by the gradient of gravitational potential and upward flows affected by the gradient of matric potential. These two flows are mainly used to simulate deep percolation occurring in redistribution processes and upward flows resulting from matric potential, respectively. The CSHMUR-EPIC model is calibrated and validated with field data for a typical arid area of northwestern China, and it is then applied for the simulation of seven irrigation scenarios. The study highlights that the upward flows aggravated by drought conditions and the under field-capacity deep percolation are remarkable enough and should not be neglected in the AWP estimation for arid and semi-arid areas with deep groundwater. The developed CSHMUR-EPIC model can effectively simulate upward flows and the under field-capacity deep percolation, and thus soil water content (SWC) both in lower and upper soil profiles, actual evapotranspiration and crop growth, resulting in an precise estimation of AWP. As upward flows and the under field-capacity deep percolation vary with irrigation schedule, the model is also helpful in exploring various irrigation schedule to obtain a sustainable agricultural water resources management.

1. Introduction

Water is a fundamental and irreplaceable resource for agricultural development and ecological systems. In recent years, under the dual impacts of climate change and human activity, water scarcity has arisen all over the world (Guo and Shen, 2016; Siska and Takara, 2015; Huo et al., 2013; Cosgrove and Loucks, 2015). This scarcity relates primarily to water required for food production rather than to water requirements for domestic or industrial purposes, which are relative minute (Rijsberman, 2006; Sauer et al., 2010; McLaughlin and Kinzelbach,

* Corresponding author at: Center for Agricultural Water Research in China, China Agricultural University, No. 17 Qinghua East Road, Haidian, Beijing, 100083, PR China.
E-mail address: huozl@cau.edu.cn (Z. Huo).

https://doi.org/10.1016/j.agwat.2018.10.024
Received 4 June 2018; Received in revised form 16 October 2018; Accepted 17 October 2018
Available online 02 November 2018
0378-3774/

2015). Globally, irrigation accounts for more than 70% of total water withdrawals and for more than 90% of total consumptive water use (Siebert et al., 2010; Scanlon et al., 2002). From a water safety and food security perspective, water resource must be managed more efficiently and agricultural water productivity (AWP) levels should be improved (Assouline et al., 2015; Amarasingha et al., 2017; Baker et al., 2012; Vaghefi et al., 2017; Masikati et al., 2014). Defined as production achieved per amount of water used, water productivity reflects the relationship between water inputs and outputs and can be adopted as a useful indicator for assessing water resource management (Pereira et al., 2012). The accurate estimation of water productivity can help guide the sustainable management of water resources and especially for those of arid and semi-arid regions where water is scarce and crop production is critical for economic development (Evans and Sadler, 2008).

Widely used for water resources management, process-based agricultural water productivity (AWP) simulations can be used as a tool for investigating and predicting crop productivity under various irrigation management conditions (Karandish and Simunek, 2016). For the simulation of water productivity, a coupled model relating soil hydrology to crop growth processes quantitatively and bridging the boundaries of the two subjects is superior to a single model (Zhou et al., 2012). As commonly used physical models, crop growth models often simulate crop growth based on empirical functions or model underlying physiological processes of crop growth in relation to a surrounding environment (Liu, 2009). Substantial crop growth models have been developed and widely used (e.g., EPIC (Williams et al., 1989), WOFOST (Hijmans et al., 1994), Cropsyst (Stockle et al., 1994), DSSAT (Jones et al., 2003) and AquaCrop (Steduto et al., 2009) over the past few decades. Of these models, the EPIC crop growth model offers high levels of simulation precision with less demanding data input requirements and thus catch the attention of hydrologists (Xu et al., 2013; Wang et al., 2014).

There are two main means of simulating the soil hydrology of an unsaturated zone: numerical solutions to the Richards equation and the soil water balance approach. Models based on the Richards equation are often restricted to evaluating small areas, and estimates generated can be highly uncertain because functional relationships applied through the Richards equation are time-consuming and difficult to measure, especially at low water content. In contrast, a soil water balance approach can be applied to large areas with little experimental data (Flint et al., 2002; Scanlon et al., 2002; Gao et al., 2017; Xue et al., 2018). As a result, almost all soil hydrology modules considered in crop growth models, such as EPIC, Cropsyst, DSSAT, AquaCrop, and so on, adopt a soil water balance approach to simulate soil water movement. In view of the indication that unsaturated hydraulic conductivity below the field capacity are so low that soil-water flows are usually assumed to be zero, most of soil water balance models such as Williams-Ritchie water balance model used in EPIC, CERES and PERFECT models (Littleboy et al., 1992), AquaCrop (Raes et al., 2009) and Hydrobal model (Bellot and Chirino, 2013) only simulate water flows during the period hydraulic conductivity in excess of field capacity (the over field-capacity redistribution as follows) but not consider water flows when hydraulic conductivity below the field capacity (the under field-capacity redistribution as follows). These models have something in common: (1) they limit percolation simulations to the 1–3 day period following saturation and (2) they neglect upward flows resulting from matric potential in soil water redistribution processes. However, the redistribution process is in fact continuous and can persist at an appreciable rate for many days or even months after precipitation or irrigation (Hillel, 1982; Kendy et al., 2003). It is considered to be a passive process that occurs in a variety of directions (i.e., downward, upward and even laterally) through soil profiles (Mendel et al., 2002; Richards and Caldwell, 1987). Although proven successful when applied to wet regions, these models do not adequately simulate soil water flows occurring in drought conditions, as crop growth is more sensitive to deep percolation and upward flows. Even low levels of deep percolation (the under field-capacity deep percolation) no longer supporting crop growth may sustainably accumulate to a considerable volume. Kendy et al., (2003, 2004) provided a method to manage the under field-capacity deep percolation and successfully estimated the long-term deep percolation occurring in Luancheng Count of the western North China Plain. Unfortunately, it cannot effectively simulate the upper half of a soil-moisture profile, causing an adverse impact on the simulation of evapotranspiration, crop production and AWP. Jones et al. (2003) indicated that continuous evapotranspiration can spur upward flows. In entering water-limited layers containing large roots, upward flows can enhance transpiration and benefit crop growth during rainless periods (Scott et al., 2008; Guswa, 2005; Lee et al., 2005; Quijano and Kumar, 2015). Without water supply for crop growth except for low frequency irrigation and tiny amount of precipitation in arid and semi-arid areas with deep groundwater, high and continuous evapotranspiration will substantially aggravate upward flows produced and the aggravated upward flows probably should not be neglected in the simulation of AWP.

In this paper, a conceptual soil hydrological model considering under field-capacity redistribution (CSHMUR) was proposed and coupled with the EPIC crop growth model to investigate the effect of the under field-capacity deep percolation and upward flows on the AWP estimation for arid and semi-arid area with deep groundwater. With field data from a typical arid area in northwestern China, the coupled AWP model (CSHMUR-EPIC model) was calibrated and validated and the simulation effects were evaluated. In addition, in order to explore the practical application in sustainable agricultural water resources management, the developed model was used in the simulation of several irrigation scenarios.

2. Materials and methods

2.1. Overview of the model

As discussed by Pereira et al. (2012), the term WP should be used rather than the term water use efficiency (WUE). The total water productivity is the ratio between the achieved yield and the water used to produce that yield. Agricultural water productivity (AWP) herein refers to the total water productivity of agricultural crops and it can be used at farm scale or regional scale. The total water use consists of actual evapotranspiration from crops and deep percolation at field scale. At regional scale, canal conveyance operational loss is also included in the total water use in addition to the water use at field. The developed CSHMUR-EPIC model is designed to simulate the farm-scale AWP and can also provide main inputs for regional scale AWP estimation. At farm scale, AWP (kg/m^3) is calculated from the following equation:

$$AWP = \frac{Y}{ET_a + D_p} \tag{1}$$

where ET_a is the actual season evapotranspiration, where D_p is deep percolation and where Y is the crop yield (kg).

The dynamic response relationship between soil water content and crop growth is central to assessing and predicting AWP. In this study, the AWP model is established by coupling a conceptual soil hydrological model considering under field-capacity redistribution (CSHMUR) and the EPIC crop growth model to take full advantage of the characteristics of these two models and to reduce the number of input parameters used. Under field-capacity redistribution is considered in the soil hydrological model by regarding soil water redistribution as the mixing of two separate and sequential water flows: downward flows affected by the gradient of gravitational potential and upward flows affected by the gradient of matric potential. Downward and upward flows are mainly used to simulate deep percolation occurring through redistribution processes and water movements due to evapotranspiration, respectively. Crop growth indicators (e.g., the leaf area index and

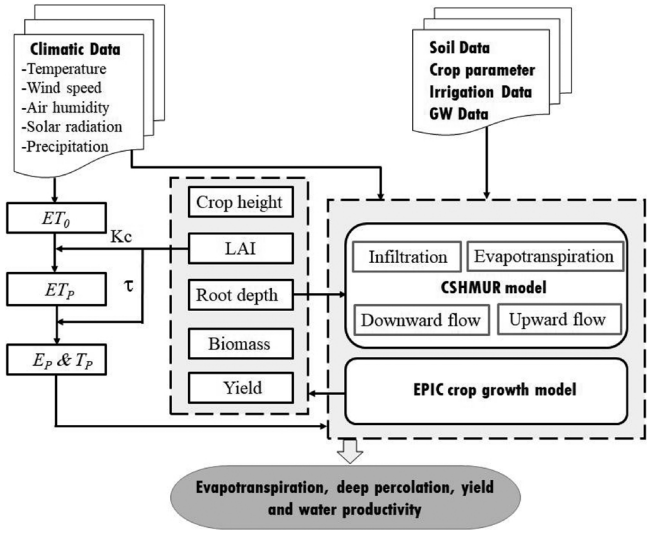

Fig. 1. Schematic diagram of coupling the conceptual soil hydrology model considering under field-capacity redistribution (CSHMUR) and the EPIC crop growth model.

root depth) the EPIC crop growth model can provide must be input into CSHMUR, and in turn, soil moisture levels simulated through CSHMUR serve as essential input data for the EPIC crop growth model. Specifically, as the main output parameters of the EPIC crop growth model, the leaf area index and root depth vary. In using the leaf area index, root depth and soil moisture level as an interface and by applying information exchange on a daily basis, these two models are coupled and a model (CSHMUR-EPIC) simulating AWP for arid and semi-arid areas with deep groundwater is developed. A schematic diagram of the coupling structure is presented in Fig. 1. The model code was written in Matlab 2014a and requires the use of Microsoft Excel data to run. Outputs of actual evapotranspiration (ET_a), deep percolation (D_p) and crop yields (Y) generated from the model are used to calculate the total agricultural water productivity AWP level (kg/m^3).

2.2. Soil hydrology

In arid and semi-arid areas with flat terrain, surface runoff on irrigated land can be assumed negligible, but processes such as those of infiltration, evapotranspiration and redistribution must be considered in relation to soil hydrology. Infiltration and redistribution processes mentioned in this paper refer to the water movement process before and after all the water entry into soil following a rainfall or irrigation event, respectively. The division is only for calculation purpose and the water flow simulated in the model is continuous process in deed as the process are simulated step by step and there is no interval between their calculations. In redistribution process, soil water movement is driven by the gradient of soil water potential, which includes gravitational potential and matric potential. As numerical solution to Richards' equation is time-consuming and the intrinsic parameters are difficult to measure, a conceptual method is explored to simulate flow process. In soil water redistribution module, water flux q is assumed as the mixing of two hypothetical components: water flux $q(g)$ affected by the gradient of gravitational potential and water flux $q(m)$ affected by the gradient of matric potential. The value of $q(g)$ is always negative, and thus $q(m)$ accounts for upward flows. To minimize computational efforts required, $q(g)$ and $q(m)$ are calculated separately and sequential for each time step, just like the calculation of ET and soil water. The soil water budget (Fig. 2) equation of a vertical soil column is expressed as follows:

$$\theta_{1,t}L_1 = \theta_{1,t-1}L_1 + P_t + I_t - q(i)_{1,t} - E_{1,t} - T_{1,t} - q(g)_{1,t} + q(m)_{1,t} \quad (2)$$

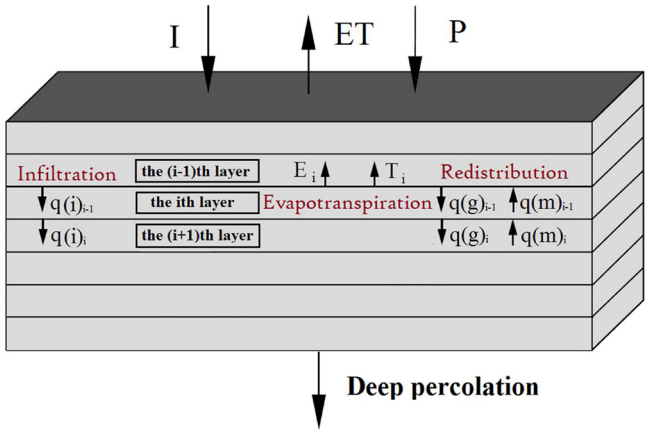

Fig. 2. Soil hydrology processes considered in the model.

$$\sum_{i=2}^{N}\theta_{i,t}L_i = \sum_{i=2}^{N}[\theta_{i,t-\Delta t}L_i - E_{i,t} - T_{i,t} + q(i)_{i-1,t} - q(i)_{i,t} + q(g)_{i-1,t} - q(g)_{i,t} + q(m)_{i,t} - q(m)_{i-1,t}] \quad (3)$$

where subscripts t, Δt and i denote time (d), the time step (1d) and the ith soil layer, respectively; where N is number of soil layers; where L is the thickness of the soil layer considered (cm); where P and I are precipitation and irrigation, respectively (cm/d); where $q(i)_i$ is the water flux (cm/d) out from the bottom of layer i in infiltration process, where $q(g)_i$ is the downward flux (cm/d) out from the bottom of layer i affected by the gravitational potential gradient in redistribution process, where the sum of $q(i)_N$ and $q(g)_N$ is taken as the occurrence of deep percolation from the simulated soil column; and where $q(m)_i$ is the upward flow flux (cm/d) from layer $i+1$ to layer i affected by the matric potential gradient in redistribution process. For areas with deep groundwater, the bottom of the soil profile is considered a free drainage boundary and $q(m)_N$ is 0. Note that the flow directions of $q(i)$ and $q(g)$ are set as downward while that of $q(m)$ is set as upward. Therefore, $q(i)$ and $q(g)$ always have positive values, and $q(m)$ appears to be negative early on and positive later on.

2.2.1. Infiltration during irrigation and precipitation events

Water distribution through a soil profile following precipitation or irrigation is simulated with a 'tipping bucket' module (Riha et al., 1994). In the module, once precipitation or irrigation occurs, water enters the soil immediately. The water first enters the uppermost soil layer and then excess water flows to deeper layers when the soil moisture level reaches saturation. The process continues in a 'tipping bucket' fashion until each layer is filled to saturation or until all of the water has been distributed. Any excess water that drains from the lowest layer $q(i)_N$ becomes part of the deep percolation process for the considered time-step.

2.2.2. Evapotranspiration

As a form of consumptive water use, evapotranspiration is the broadest term used after precipitation and irrigation (Morillas et al., 2013). As transpiration sustains crop growth needs, the model partitions evapotranspiration (ET) into evaporation and transpiration to simulate evapotranspiration processes. The FAO-56 Penman-Monteith method (Allen et al., 1998) is used to compute the reference crop potential evapotranspiration ET_0 (mm/d) value.

$$ET_0 = \frac{0.408\Delta(R_n - G) + \gamma\frac{900}{T+273}u_2(e_s - e_a)}{\Delta + \gamma(1 + 0.34u_2)} \quad (4)$$

where Rn is the net radiation flux at the reference grassland (alfalfa) surface (MJ /(m^2. d)), where G is soil heat flux (MJ /(m^2. d)), where T is mean air temperature (°C), where U_2 is wind speed (m s^{-1}) at a height

of 2 m, where e_s is saturation vapor pressure (kPa), where e_a is the actual vapor pressure level (kPa), where Δ is the slope of the vapor pressure curve (kPa $^{\circ}C^{-1}$) and where γ is the psychrometric constant (kPa $^{\circ}C^{-1}$).

The potential evapotranspiration of crop ET_P is calculated as:

$$ET_p = K_c \times ET_0 \tag{5}$$

where K_c is the crop coefficient, and it is worth noting that K_c in this study is not necessarily the same as the crop coefficient in the traditional sense (K_c) as described by Allen et al. (1998).

K_c is important for calculating ET_P for the concerned crop and changes with crop growth. Sau et al. (2004) and DeJonge et al. (2012) have successfully used the following formula for the calculation of K_c:

$$K_c = 1.0 + (K_{c\max} - 1.0) \times \frac{LAI}{LAI_{\max}} \tag{6}$$

where LAI is the leaf area index, where $LAI_{\max}$ is the maximum LAI value and where $K_{c\ max}$ is K_c with the largest possible LAI. A value of 1.1 for $K_{c\ max}$ is recommended according to the research results of Sau et al. (2004), and in this paper the $K_{c\ max}$ value is set to 1.1. The equation defines the ET_P of bare wet soil (with a zero LAI value) as the same as the ET_P value of the reference crop (ET_0; 0.12 m tall and LAI of 2.88).

Potential evapotranspiration (ET_P) includes potential soil evaporation (E_P) and potential transpiration (T_P). The ratio of Ep to T_P is shaped by the developmental stage that a leaf canopy occupies and it can be expressed as a function of LAI. Ritchie (1972) partitioned ET_P into Ep and T_P with the following equation:

$$E_P = ET_P \exp[-(K_b)(LAI)] \tag{7}$$

$$T_p = ET_p - E_P \tag{8}$$

where K_b is the dimensionless canopy extinction coefficient. For crops in general, Ritchie (1972) used a K_b value of 0.85 while Belmans et al. (1983) used a K_b value of 0.6. Sau et al. (2004) found that a value of close to 0.5 may be more adequate for further solar radiation analyses, and it was proved to exhibit good performance for the simulation of evapotranspiration, biomass and yields (López-Cedrón et al., 2008; DeJonge et al., 2012).

Evaporation can drive water from as deep as 3 m in a profile, though most water is removed from surficial areas. Assuming that transpiration equals to root water uptake loss and transpiration removes water from all layers containing plant roots. The potential volume of soil surface water uptake to any root depth is estimated with the function (Novark, 1987).

$$U_{(z)} = T_p \frac{1 - \exp\left[-\delta\left(\frac{z}{z_r}\right)\right]}{1 - \exp(-\delta)} \tag{9}$$

where $U_{(z)}$ is the total water uptake rate (cm/d) from a ground surface to depth z (cm), where z_r is root depth (cm), and where δ is a water use distribution parameter. A δ value of 3.64 is adequate for corn (Novark, 1987), and this value is used for all crops in our model. The potential water uptake from layer i can be calculated as the difference between U values at layer boundaries:

$$T_{p(i)} = u^t_{f(i)} T_p \tag{10}$$

$$u^t_{f(i)} = \left[\frac{1}{1 - \exp(-\delta)}\right]\left\{\exp\left[-\delta\left(\frac{z_{1(i)}}{z_r}\right)\right]\left[1 - \exp(-\delta\frac{z_{2(i)} - z_{1(i)}}{z_r})\right]\right\} \tag{11}$$

where $z_{1(i)}$ and $z_{2(i)}$ are the depth of the upper and lower boundaries of soil layer i, respectively; $T_{p(i)}$ is the potential water uptake from layer i; $u^t_{f(i)}$ is the water uptake ratio of layer i to the whole root zone, and the sum of $u^t_{f(i)}$ values for all layers of the root zone is equal to 1.0. Kendy et al. (2003) used the same equation to calculate $u^e_{f(i)}$ and to allocate evaporation to soil layers by substituting root depth for soil-layer depth and by setting 10 as the δ value, and results showed the reasonableness as evaporation is more heavily concentrated close to surface soils than transpiration. In this paper, the δ value for evaporation was also set as 10.

$$E_{p(i)} = u^e_{f(i)} E_p \tag{12}$$

where $E_{p(i)}$ is the potential volume of soil evaporated from layer i and where $u^e_{f(i)}$ is the evaporation fraction of layer i to all soil layers.

The actual evaporation and transpiration from layer i are closely related to water conditions and can be computed as

$$E_{a(i)} = K_{r(i)} \times E_{p(i)} \tag{13}$$

$$T_{a(i)} = K_{s(i)} \times T_{p(i)} \tag{14}$$

where $E_{a(i)}$ and $T_{a(i)}$ are the actual soil evaporation and transpiration from layer i, respectively and where $K_{r(i)}$ and $K_{s(i)}$ are the water stress coefficients of evaporation and transpiration, respectively.

The water stress coefficients for each layer are written as the following equations (Raes et al., 2009):

$$K_r = \begin{cases} \exp\left(2.5\frac{\theta - \theta_{fc}}{\theta_{fc} - \theta_{wp}}\right) & \theta < \theta_{fc} \\ 1 & \theta \geq \theta_{fc} \end{cases} \tag{15}$$

$$0 \leq K_s = 1 - \frac{\exp(D_{rel} \times f_{shape}) - 1}{\exp(f_{shape}) - 1} \leq 1 \tag{16}$$

$$D_{\text{rel}} = 1 - \frac{\theta - \theta_{wp}}{(1 - p)(\theta_{fc} - \theta_{wp})} \tag{17}$$

where θ_{fc} and θ_{wp} are the volumetric SWC at field capacity and the wilting point (cm^3/cm^3), respectively; D_{rel} (≤ 1) is relative water depletion, f_{shape} is the shape factor of the K_s curve, and p is the fraction of readily available soil water relative to the total volume of available soil water.

2.2.3. Soil water redistribution

2.2.3.1. Downward flows affected by the gradient of gravitational potential in redistribution. Assuming that no incoming or outgoing water fluxes occur other than those produced by a unit gradient at the bottom of a layer, outflows from a layer can be expressed according to the conservation of mass as

$$L\frac{d\theta}{dt} = -K(\theta) \tag{18}$$

where L is layer thickness (cm), where θ is the average volumetric SWC of the layer (cm^3/cm^3), where t is time (d) and where K is unsaturated hydraulic conductivity (cm/d). The equation is put forward by Steenhuis and van der Molen (1986) and then is successfully applied to groundwater recharge estimation for western North China Plain (Kendy et al., 2003). According to their finding, Eq. (18) can be solved from an exponential relationship between K and θ, which involves few parameters such that

$$K(\theta) = K_s \exp(-\alpha\frac{\theta_s - \theta}{\theta_s - \theta_d}) \tag{19}$$

where Ks is saturated hydraulic conductivity (cm^3/day), where θ_s is the volumetric SWC of a soil layer at saturation (cm^3/cm^3), where θ_d is the volumetric SWC of dry soil (cm^3/cm^3), where the value of θ_d is half that of θ_{wp} (Allen et al., 1998; Raes et al., 2009; Ritchie, 1996; Sharpley and Williams, 1990) and where α is an empirical parameter. For homogeneous soils, α is approximately valued at 13 (Bresler et al., 1978; Steenhuis and van der Molen, 1986); for heterogeneous soils, α can be as large as 16 (Russo and Bresler, 1980; Kendy et al., 2003). By substituting Eq. (18) into Eq. (19) and by integrating over time step Δt, the SWC of a single layer after infiltration can be obtained

$$\theta_t = \theta_s - \frac{\theta_s - \theta_d}{\alpha} \ln\left[\frac{\alpha K_s \Delta t}{L(\theta_s - \theta_d)} + \exp(\alpha \frac{\theta_s - \theta_{t-\Delta t}}{\theta_s - \theta_d})\right] \quad (20)$$

Downward flow flux out of a layer over one time-step represents the difference between soil water stored as calculated from Eq. (20) and that measured prior to calculation. Then, calculations shift from the present layer to the underlying layer. Two conditions of water flux entering into the deeper layer are considered: (1) at the start of the time-step and (2) at the end of the time-step. For either condition, calculations generate considerable errors, especially in precipitation or irrigation day. To limit simulation errors, soil water content observed at the end of the time-step for the two cases are computed separately, and the average SWC is taken as the eventual SWC value of this process. As a result, the downward flow flux from each layer is calculated for one time-step.

As deep percolation occurs in both infiltration and redistribution processes, the total deep percolation in one time-step is the sum of the downward flux from the bottom of the soil profile calculated from the 'tipping bucket' module and from the 'downward flow' module.

2.2.3.2. Upward flows affected by the gradient of matric potential in redistribution. In arid and semi-arid areas, it is common for soil water to flow upward due to low moisture levels in the upper layer soil. Subroutine upward flows are thus determined to compute changes in volumetric SWC resulting from the upward movement of soil water through the profile. The upward flow of water from soil layers is calculated based on capillary flow theory (Jones et al., 1986), according to which upward flow is approximated from a normalized soil water diffusion concept based on a daily time-step. Water content is normalized to the SWC at the wilting point where an assumption is made that the diffusivity of all soils is D_0. The assumed average diffusivity above the SWC at the wilting point of two adjacent layers is a function of the normalized SWC for all soils (Ritchie, 1996).

$$D_i = D_0 \times \exp\left[\beta \times \left(\frac{\theta_i - \theta_{wp(i)}}{2} + \frac{\theta_{i+1} - \theta_{wp(i+1)}}{2}\right)\right] \quad (21)$$

where D_i is the average diffusivity value (cm^2/d) of layer i and layer $i+1$ where the SWC is above the wilting point, where D_0 is the diffusivity value (cm^2/d) where the SWC reaches the wilting point, and where β is an empirical parameter. When D_i is greater than 100, it is limited to 100 cm^2/d. Ritchie (1996) found a D_0 value of 0.88 and a β value of 35.4 by fitting data given by Rose (1968). Suleiman and Ritchie (2003) found an exponential relationship between diffusivity and SWC, and a D_0 value of 2.7 and a β value of 27.5 were found when we fitted the data with Eq. (21).

The upward flow flux $q(m)_i$ from layer $i+1$ to layer i is calculated as:

$$q(m)_i = D_i \times \frac{[(\theta_{i+1} - \theta_{wp(i+1)}) - (\theta_i - \theta_{wp(i)})]}{0.5 \times (L_i + L_{i+1})} \quad (22)$$

When the normalized SWC of layer i is greater than that of layer $i+1$, $q(m)_i$ is a negative value and water moves downward.

2.3. Crop growth processes

The EPIC (Erosion-Productivity Impact Calculator) crop growth model was developed to estimate soil productivity as it is affected by erosion throughout the U.S. It simulates all crops with one crop growth model using unique parameter values for each crop. Processes simulated include the leaf area index; root growth; conversion to biomass; the division of biomass into roots; the above ground mass; and economic yields. In the model, the phenological development of a crop is based on daily heat unit accumulation patterns. A crop starts to grow when the average daily air temperature exceeds the base temperature and it can be harvested when accumulated heat units reach potential heat units required for maturity. The interception of solar radiation is estimated as a function of *LAI*, which depends on the crop species, heat units and crop stress. Potential biomass and yields are respectively estimated using the concept of Biomass-Energy Ratio and harvest index (economic yield/aboveground biomass). Potential growth is constrained by the minimum of five stress factors (water, nitrogen, phosphorus, temperature, and aeration). A more detailed description of the EPIC crop growth model can be found in Williams et al. (1989).

2.4. Model performance evaluation method

To quantitatively evaluate the model's performance, the coefficient of determination (R^2), the root mean square error (*RMSE*), the mean relative error (*MRE*) and the Nash-Sutcliffe modeling efficiency (*NSE*) value (Nash and Sutcliffe, 1970; Moriasi et al., 2007) were computed as shown in Eqs. (23)–(26), respectively:

$$R^2 = \frac{[\sum_{i=1}^{n}(S_i - S_{ave})(M_i - M_{ave})]^2}{\sum_{i=1}^{n}(S_i - S_{ave})^2 \sum_{i=1}^{N}(M_i - M_{ave})^2} \quad (23)$$

$$RMSE = \sqrt{\frac{1}{n}\sum_{i=1}^{n}(M_i - S_i)^2} \quad (24)$$

$$MRE = \frac{1}{n}\sum_{i=1}^{n}\left|\frac{M_i - S_i}{S_i}\right| \times 100\% \quad (25)$$

$$NSE = 1 - \frac{\sum_{i=1}^{n}(S_i - M_i)^2}{\sum_{i=1}^{n}(M_i - M_{ave})^2} \quad (26)$$

where n is the total number of measurements; where S_i and M_i are the ith simulated and measured values (i = 1,2, …, N), respectively; and where S_{ave} and M_{ave} are the averages of the simulated and measured values, respectively. Generating R^2 and *NSE* values of closer to 0 and *RMSE* and *MRE* values of approximately 1 shows that the model is performing well. Positive *NSE* values denote that the model can be applied, and the model is inappropriate to use when *NSE* values are far below 0.

2.5. Experimental data for model testing

The Yingke Irrigation District (YID) (38°50–38°58 N, 100°17–100°34E) located in middle oasis of the Heihe River Basin in northwestern China (Fig. 3) is selected as our case study area. It is the third largest irrigation district of the middle oasis and spans 17.4 km from east to west and 14.2 km from south to north, covering an area of 192.2 square kilometers. At a 1/70-1/1000 natural gradient, the terrain in the area is relatively flat, and elevations vary between 1456 m and 1600 m from northeast to southwest. The local climate of the YID is arid continental. Annually, average temperatures reach 6.5–7.0 °C and a minimum of −28 °C and a maximum of 33.5 °C, and average precipitation levels reach 125 mm while the local reference crop evapotranspiration level (ET_o) is approximately 1200 mm.

As a major part of the middle oasis, which forms an important grain production base, the YID requires approximately 175 million m^3 of irrigation water per year, accounting for 10% of water requirements of the middle oasis and for more than 90% of water used in the YID. In the YID, crops grown mainly include corn, wheat and vegetables and a few of forest, grass and other crops. After crop pattern adjustments were made in 2000 (Shi et al., 2011), corn became the main crop grown, accounting for 78% of all crops grown in the area. For these crops, rainfall levels are too low to meet crop water consumption needs, and irrigation water mainly originates from Heihe River stream flows and is supplemented by groundwater. For irrigation purposes, the local government and farmers have built a large canal network consisting of one main canal, 2 sub-main canals, 27 secondary canals, 173 lateral canals and more than 1000 sub-lateral canals. The canals span 1119.1 km, and

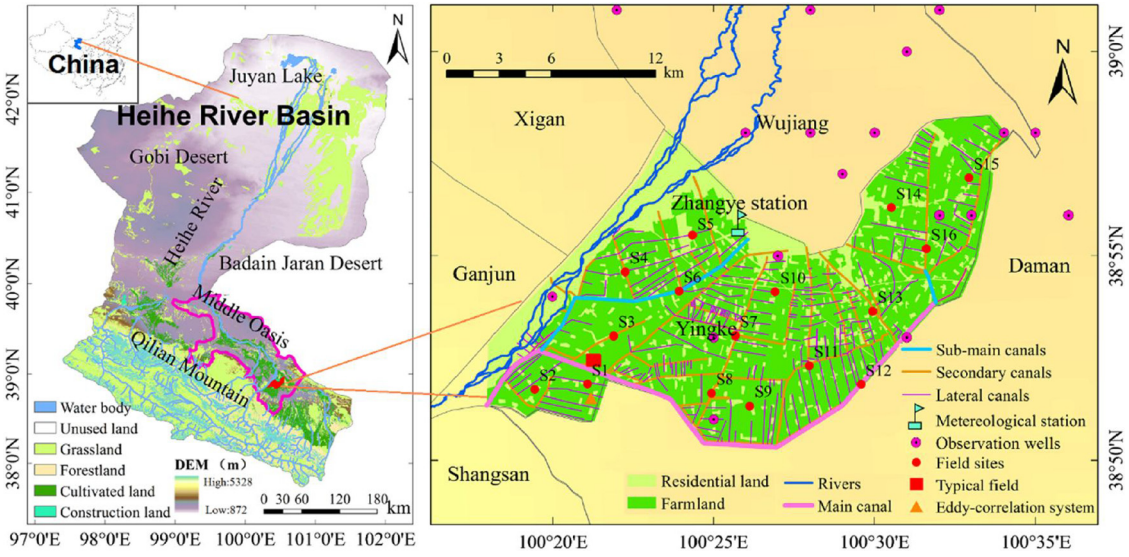

Fig. 3. Location of the Yingke Irrigation District and distribution of the observation points.

most have been lined since the application of water saving practices in 2000 (Jiang et al., 2015). Yingke main canal, the only main canal in YID, diverts water directly from the Heihe River and supplements the canal network.

2.5.1. Field experiment

Field experiments were carried out at 16 field sites from 2012 to 2013 and a typical field in 2012 (Fig. 3). The 16 field sites (S1–S16) distributed across different areas of the YID were arranged based on digital soil, land use, crop and canal network maps and they covers four soil types (from 0 to 80 cm to 80–140 cm: silt loam-silt loam, silt loam-sandy loam, silt loam-loam and loam-loam), three crop types (corn, wheat and cabbage) and different irrigation volume. Besides, a field covering different soil types was added to our experiment, and four points (T1–T4) located in this typical field we calls observation points having the same crop types (corn) and irrigation volume represents four types of soil. In 2012, corn was planted in all 16 field sites and in the typical field; in 2013, wheat was planted in S5 and S7 and cabbage was grown in S10. Among the 16 field sites, S2, S5 and S10 were used to represent corn, wheat and cabbage, respectively, which are the main crops grown in the YID. Soil moisture and crop growth indicators including the leaf area index and dry above-ground biomass were recorded every 2 weeks at the 16 field sites and every 1 week at the four observation points of the typical field. Soil moisture was measured using the time domain reflectometry method, and undisturbed soil samples were collected via the cutting ring method using 7 layers of equal thickness to a depth of 140 cm. Using a Malvern laser particle size analyzer called the Mastersizer 2000, soil samples were analyzed and soil texture data were obtained. For crop growth indicators, the leaf area index (LAI) and dry above-ground biomass (D-AGB) values were measured by AccuPAR-LP80 directly and by drying the above-ground biomass to a constant weight at 75 °C. An irrigation schedule and crop growth period (Table 1) were applied according to recommendations made by the local water conservancy department, farmers and a number of researchers.

2.5.2. Data collection

Daily meteorological data including those for rainfall, maximum and minimum temperature, wind speed, sunshine duration and relative humidity levels for the Zhangye weather station (100°26′E, 38°56′N, 1482.7 m) were downloaded from the China Meteorological Data Service System (http://cdc.nmic.cn/home.do). While neglecting spatial variations, data collected at the Zhangye weather station can be regarded as representative meteorological of the entire area, as the station is positioned within the YID (Fig. 3).

Dozens of groundwater monitoring wells (Fig. 3) were found within and around the YID, and groundwater depths monitored by these wells in 2004 were available. Via Inverse Distance Weighting (IDW), the monitored depth was interpolated and the spatial distribution of groundwater depth in the YID (Fig. 4) was determined. For nearly the entire YID, groundwater depths in 2004 exceeded 4 m. The unrestrained use of groundwater resources has resulted in a gradual decline of the water table in recent years and groundwater depth will continue to increase over the next 10 years (Chen et al., 2016; Li et al., 2017a). Therefore, the YID can be considered an area with deep groundwater and it is reasonable to omit phreatic water evaporation in the simulation of soil water cycles in 2012 and 2013.

To test the model's performance in actual evapotranspiration simulation, flux data measured from an eddy-correlation system (Fig. 3) were obtained from the Western Database (http://www.heihedata.org/c). An eddy-correlation system was installed at a corn area site close to the S1 and S2 sites, and within these sites irrigation schedules used are quite similar. The EC data cover the period running from May 30 to September 21, 2012, and were processed using Edire software

Table 1
Representative crop growth period and irrigation schedule in experimental plots.

Crop type	Crop growth period			Irrigation Schedule				
	Sowing	Seed germination	Harvest	Frequency	irrigation data			
wheat	Apr 1	Apr 20	Jul 20	3	Apr 22	May 24	Jun 23	
corn	Apr 20	May 7	Sept 22	4	May 26	Jun 23	Jul 20	Aug 18
cabbage	Mar 20		May 30	6	May 22	Apr 22	May 15	
	Jun 20		Aug 30		Jun 23	July 12	Aug 18	

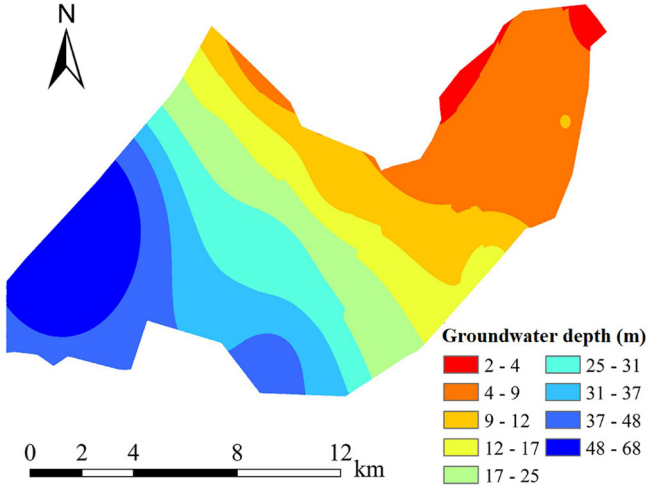

Fig. 4. Groundwater depth of the Yingke Irrigation District in 2004.

developed by the University of Edinburgh (Liu et al., 2016). Using the Bowen Ratio-equilibrium energy balance closure method (Consoli and Papa, 2013), we corrected EC data to improve measurement precision levels.

3. Results and discussion

3.1. Model calibration and validation

Soil and crop parameters were calibrated and validated by comparing simulated and measured soil water content (*SWC*), actual evapotranspiration (ET_a), leaf area index (*LAI*) and dry above-ground biomass (*D-BAG*) values. From field observations and collected data, S5, S7, S10 for 2013 and other field sites for 2012 were used to calibrate soil and crop parameters (corn, wheat and vegetables), and S5, S7, S10 in 2012 were used to validate the calibrated parameters (soil and corn growth parameters). As only one-year data for wheat and cabbage crops were collected, crop growth parameters of these two forms were only calibrated and not validated. In addition, four observation points (T1, T2, T3 and T4) located in the typical field were used for supplementary validation. In general, S2 for 2012, S5 for 2012, and S5 and S10 for 2013 were selected as representative sites of corn, wheat and vegetable growth, respectively, and S2 was used to analyze simulation effects of soil hydrology. Calibrated values of crop parameters included in the EPIC crop growth model for corn, wheat and cabbage and soil parameters at S2 are shown in Tables 2 and 3, respectively.

As is shown in Fig. 5, simulations of LAI and D-BAG for corn correspond well with measurements made during calibration and validation. For the LAI of corn, RMSE and MRE values were measured as 0.429 and 8.2%, respectively, while R^2 and NSE values respectively reached 0.877 and 0.846 during calibration; RMSE and MRE values collected during validation were found to be larger than those collected during calibration and R^2 and NSE values decreased, denoting satisfactory performance not fully meeting that of the calibration. Regarding D-BAG values for corn during calibration and validation, R^2, RMSE, MRE and NSE were measured as similar at 0.912, 2.877 t/ha, 11.6%, and 0.799 during calibration and at 0.920, 2.778 t/ha, 17.7% and 0.902 during validation. In addition, simulated LAI for wheat and cabbage values satisfactorily matched the measured values (Fig. 6), generating R^2 values of 0.904 and 0.561, respectively, RMSE values of 0.397 and 0.715, respectively, and NSE values of 0.792 and 0.518, respectively.

The simulated SWC values show good agreement with the values measured from various field sites covering four soil types, three crop types and different irrigation schedules during calibration and validation (Figs. 7 and 8). Fig. 9 and Table 4 indicated that the model provided good performance in the SWC simulation for all the layers. In terms of average SWC values for the whole profile, the statistic suggesting that the simulation effects of whole profile was superior to that of layered.

Table 2
Calibrated values of the crop parameters in EPIC crop growth model for corn, wheat and cabbage.

Crop parameters	Corn	Wheat	Cabbage
Minimum temperature for plant growth, T_b/°C	8	2	0
Optimal temperature for plant growth,T_0/°C	25	22	18.2
Biomass-Energy Ratio, *BE*/(kg ha^{-2}) (MJ m^{-2})$^{-1}$	40	37	19
First point on optimal leaf area development curve, *ah1*	15.05	15.01	25.23
Second point on optimal leaf area development curve, *ah2*	50.95	50.95	40.86
Fraction of growing season when leaf area declines, *DLAI*	0.8	0.8	1
Leaf area index decline rate parameter, *RLAD*	0.8	0.75	0.8
Maximum crop height, H_{max}/cm	200	85	25
Maximum potential leaf area index, LAI_{max}	4.8	4.8	3.5
Maximum root depth, RD_{max}/cm	140	140	120
Harvest index, *HI*	0.48	0.48	0.8
Lower limit of harvest index, *WSYF*	0.38	0.38	0.01
Total potential heat units required for crop maturation, *PHU*/°C	2100	1800	1800

3.2. Evaluation of model performance

3.2.1. Evapotranspiration

The simulated ET_a at S2 was compared to the measured ET_a close to S2 with an eddy-correlation system for evaluating modeling performance. The results show that the simulated ET_a values are basically consistent with the measured values with the exception of values measured for several days of the initial stage and for rainy days (Fig. 10). Evaporation, the main component of evapotranspiration in initial stages, is very sensitive to water condition. Located away from eddy-correlation system, the irrigation schedule of S2 was not exactly the same. Diverse irrigation practices between in S2 and in the position eddy-correlation system located resulted in different water conditions, which can be account for the discrepancy of ET_a in initial stages. In general, large volumes of invalid data will be generated from measurements of eddy-correlation systems in rainy days, causing the measured ET_a values lower than the actual values. Even so, R^2, MRE and NSE results still, respectively, reached values of 0.519, 19.1% and 0.378. For the crop growth period, the simulated ET_a was 631 mm, which was similar to the results of other studies. Taking studies of the Zhangye Oasis as an example, Zhao et al. (2010), Li et al. (2012), Hochmuth et al. (2015) and Jiang et al. (2015) estimated maize ET_a values of 618 mm, 567 mm, 668 mm and 664–699 mm, respectively. Thus, evapotranspiration was effectively simulated via the model.

As the main component of soil hydrology, evapotranspiration (ET) plays a key role in agricultural water cycles. In agricultural areas, evapotranspiration (ET) represents the main source of consumptive water use, and it includes the productive consumptive use of water T (crop transpiration) and the non-productive consumptive use of water E (soil evaporation) (Pereira et al., 2012). The water productivity model separates ET into E and T to lessen confounding effects of the non-productive consumptive use of water (E), which is important especially when ground cover is incomplete in initial stages or as a result of sparse planting practices (Raes et al., 2011). Daily potential and actual evaporation (E_p and E_a) together with potential and actual transpiration (T_p and T_a) were calculated using the model, and simulation results for S2 for the year 2012 are shown in Fig. 11. Simulation results indicated that water stress limited water consumption and the constrained effect on evaporation and transpiration appeared an apparent difference, with

Table 3
Soil texture and the corresponding calibrated soil water movement parameters at S2.

Soil depth	Clay (%)	Silt (%)	Sand (%)	θ_s (cm^3/cm^3)	K_s (cm/day)	θ_{fc} (cm^3/cm^3)	θ_{wp} (cm^3/cm^3)
0–20 cm	10.79	49.08	40.14	0.4	19	0.33	0.14
20–40 cm	14.56	57.98	27.47	0.4	18	0.36	0.16
40–60 cm	9.42	51.55	39.03	0.4	14	0.33	0.15
60–80 cm	10.37	54.48	35.15	0.41	20	0.34	0.14
80–100 cm	10.71	50.96	38.32	0.4	10	0.33	0.14
100–120 cm	10.29	47.72	41.99	0.4	10	0.31	0.13
120–140 cm	9.86	44.47	45.67	0.4	19	0.31	0.12

$E_a/E_p = 0.33$ and $T_a/T_p = 0.98$. The relatively low non-productive consumptive water use (E_a) and high productive consumptive water use (T_a) levels found show that the irrigation schedule used for S2 are reasonable and that irrigation levels have satisfied crop growth demand. In the crop growth period, the simulated total actual evapotranspiration (ET_a) level reached 631 mm and the simulated T_a accounted for 80% of it.

3.2.2. Deep percolation

Deep percolation was simulated based on 'tipping bucket' module of the infiltration process and the 'downward flow' module of the redistribution process. Although deep percolation is critical in many soil hydrological settings, it seems fair to conclude that this hydrological flux is difficult to measure (Seyfried et al., 2005). In this paper, soil water budget was used as an analytical tool to evaluate deep percolation simulation results. The components of water budget for the 0–140 cm soil profile at S2 in 2012 are shown in Fig. 12. It can be find that the simulated soil water storage levels fit well with the measured values and the corresponding statistical indices are shown in Table 4. According to the principle of water budget, the deep percolation simulated in the AWP model is trustworthy because of the well simulated evapotranspiration and soil water storage

S2, despite receiving only 113 mm of precipitation in the crop growth period, percolated 482 mm of water from the soil profile because too much irrigation water was added to the soil (907 mm). Jiang et al. (2015) estimated that deep percolation of YID under 655–898 mm irrigation level range from 250 to 437 mm from the SWAP model, which is based on numerical solutions to the Richards equation. As excess water flows from the bottom of the soil profile when irrigation levels exceeds soil profile capacities, deep percolation simulated

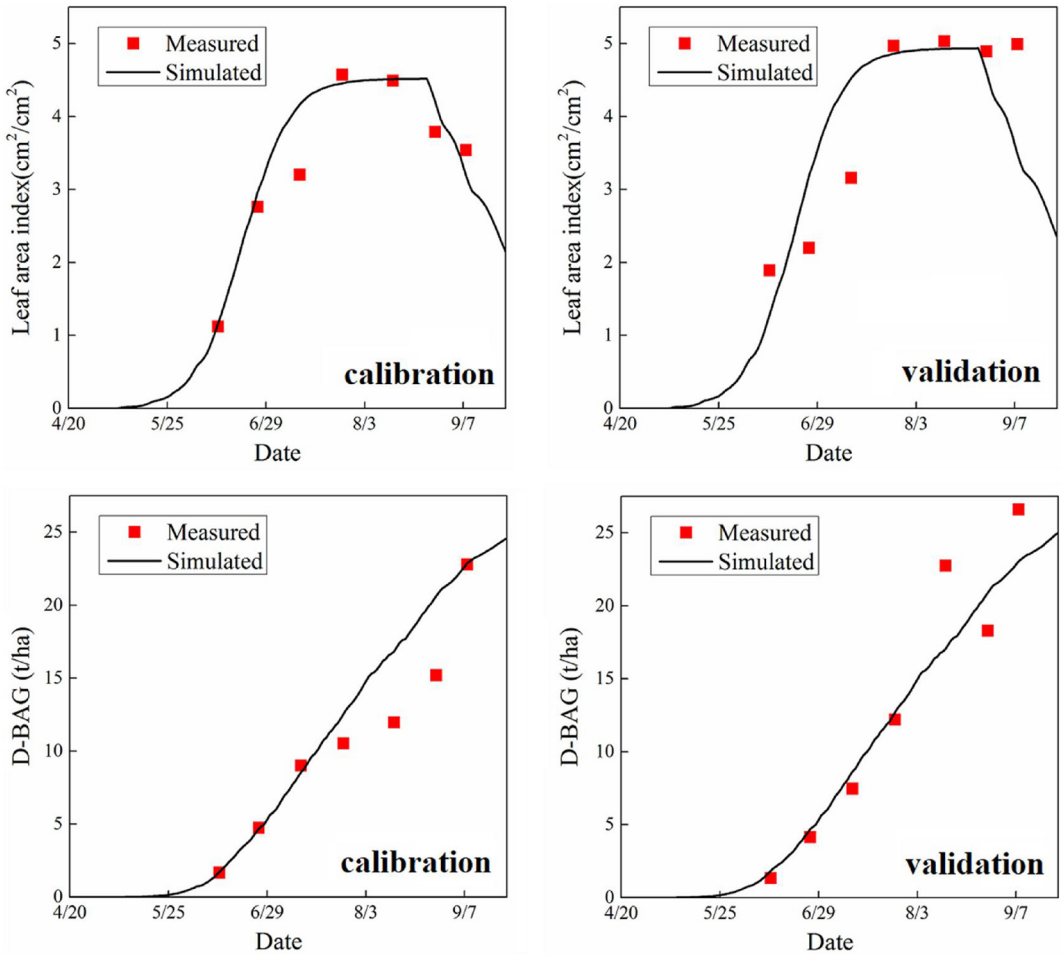

Fig. 5. Simulated versus measured leaf area index (*LAI*, a and b) and dry above ground biomass (*D-AGB*, c and d) for corn during model calibration (a and c) and validation (b and d).

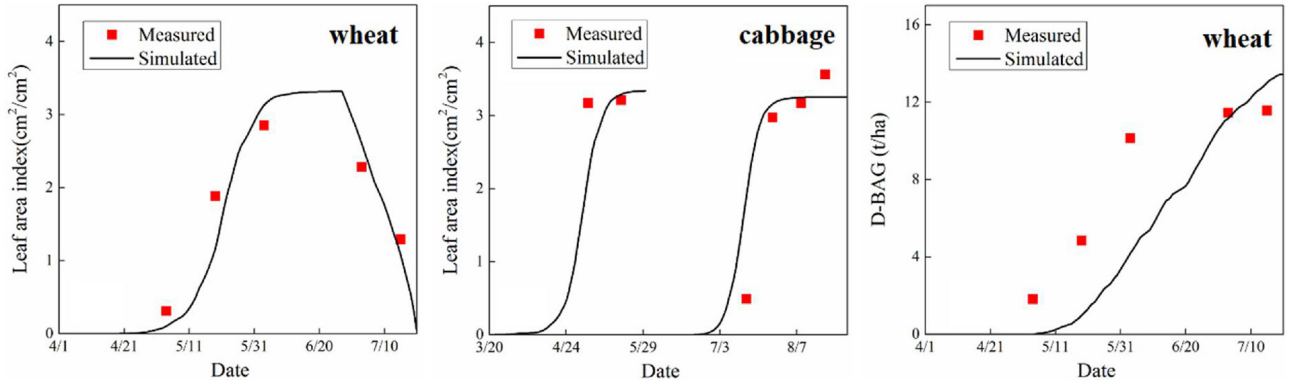

Fig. 6. Simulated versus measured leaf area index (LAI) for wheat and cabbage and dry above ground biomass (D-AGB) for wheat.

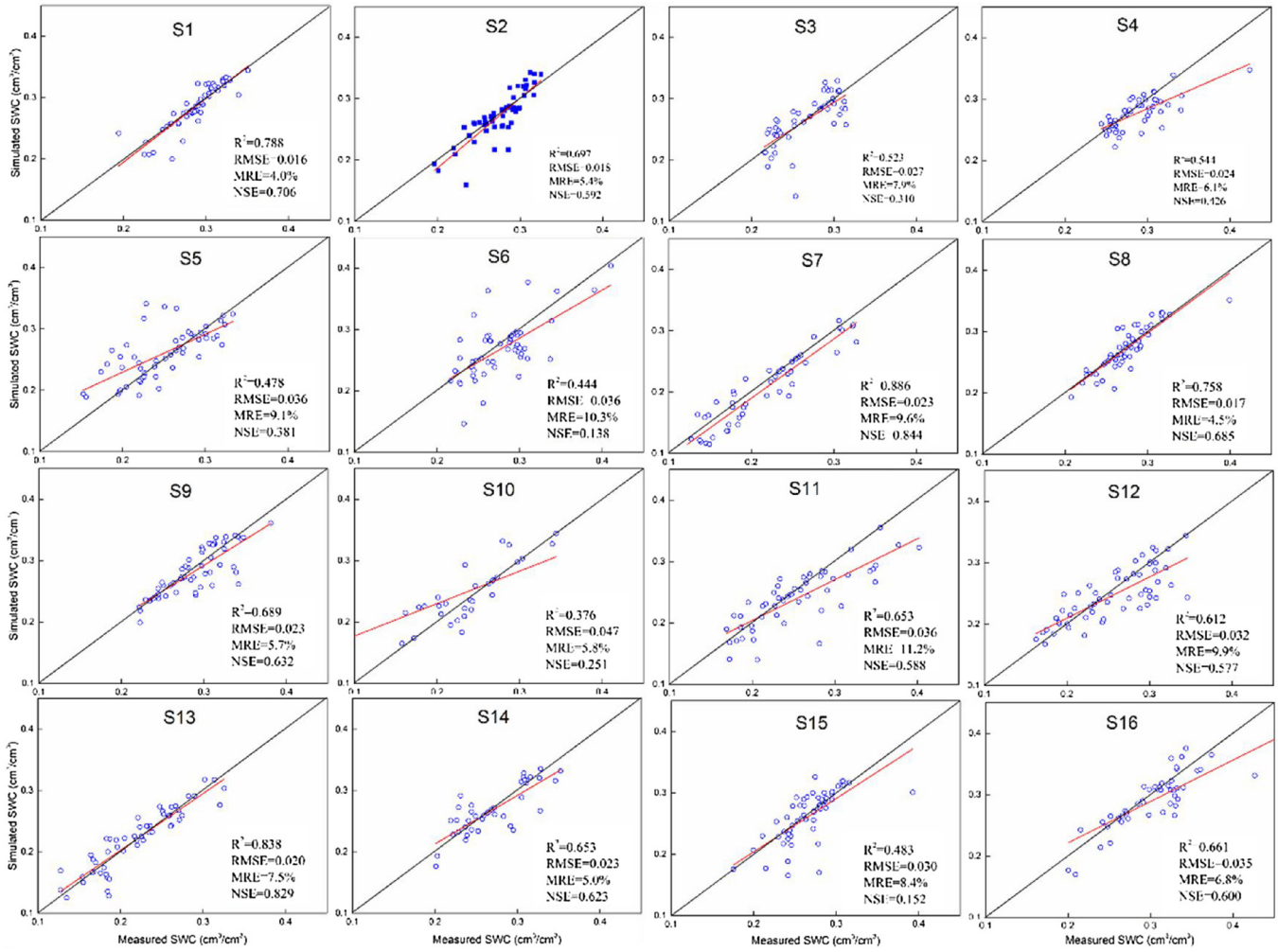

Fig. 7. Simulated vs measured SWC in 16 field sites during model calibration.

through SWAP under the 907 mm irrigation level was roughly 470 mm, which is very close to our value.

Deep percolation rates increased quickly on days of irrigation and decreased in subsequent days due to water consumption (Fig. 12). According to our simulation results, cumulative deep percolation produced in the period SWC exceeds field capacity (the over field-capacity deep percolation) was 397 mm and that produced in the period SWC is below field capacity (the under field-capacity deep percolation) reached 85 mm. The 397 mm simulated over field-capacity deep percolation is basically the same as the 350–406 mm total deep percolation estimation of Li et al. (2017b), who simulated deep percolation for maize crops of the Zhangye Oasis with a traditional conceptual soil hydrological model. The simulated 85 mm under field-capacity deep percolation was neglected in the traditional conceptual model and accounted for more than 2/3 of precipitation (113 mm). Thus, the under field-capacity deep percolation is remarkable and should not be neglected especially in the simulation of AWP for arid areas, which is in line with the findings of Kendy et al. (2003). Comparisons drawn between these three models show that the CSHMUR model can overcome the deficiency of traditional conceptual hydrological models in the

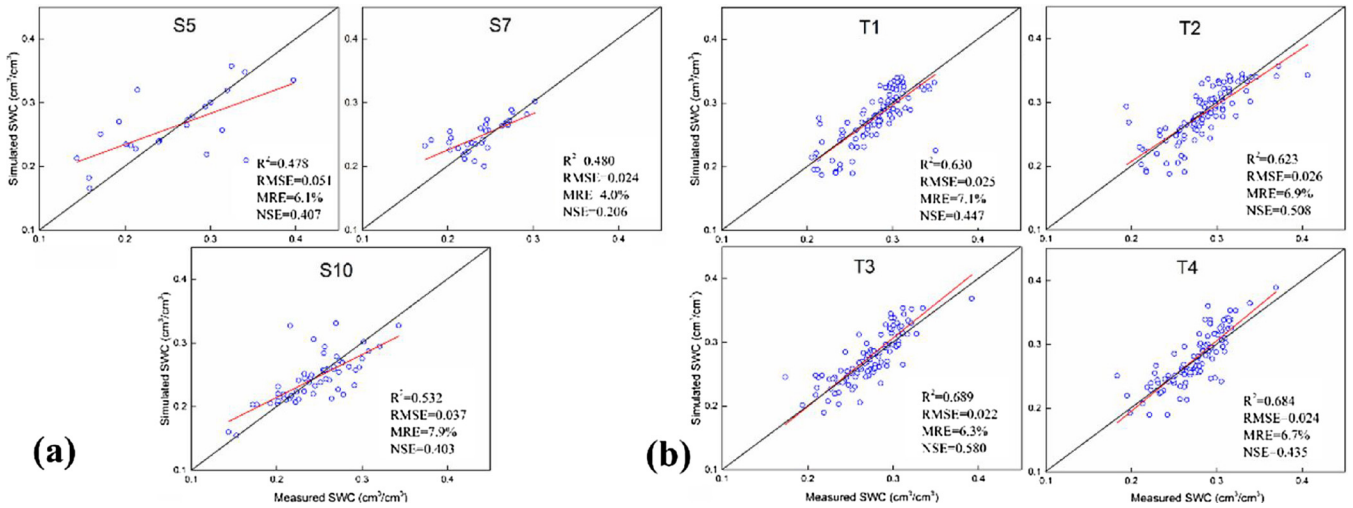

Fig. 8. Simulated vs measured SWC in 3 field sites (a) and 4 observation points (b) in the typical field during model validation.

simulation of under field-capacity deep percolation and give an estimation that is as good as the models based on numerical solutions to the Richards equation provide.

3.2.3. Soil water redistribution module that combines downward and upward flows

The soil water redistribution module that mixes downward and upward flows is proposed for capturing the continuous redistribution process. Water flow in redistribution process is assumed as the mixture of two separate and sequential flows: downward flows affected by the gravitational potential gradient and upward flows affected by the matric potential gradient.

The advantages in deep percolation have been discussed in the above section. Apart from deep percolation, water flows caused by matric potential gradient also restrict simulations of soil water redistribution in arid and semi-arid areas. Evapotranspiration spurs upward flows as it attributes to matric potential gradient (Jones et al., 2003) and drought conditions will aggravate the flows produced. If there is no gravitational potential gradient, the matric potential gradient will be the only driver of water flows and its generation is dependent on water content variations between adjacent layers. Simulation results implied that water consumed as evaporation or transpiration varies with soil depth, and the upper layer has lost more water than the lower layer (Fig. 13). In arid and semi-arid areas with deep groundwater, soil water cannot be timely supplemented and continuously high levels of evapotranspiration aggravates the matric potential gradient, thus driving upward flows that can be effectively used for crop growth. Of course, gravitational potential gradient also changes water storage levels, but the consequent variations across different layers were always found to be similar except in a very short period immediately following low irrigation and precipitation. This exception only occurs if irrigation or precipitation is not high enough to allow all layers to reach saturated water content levels and can be attributed to the assumption of the 'tipping bucket' infiltration routine. In this short period, matric potential gradient drives downward flows, and even so, water flows are mainly simulated from the downward flow module as the flow flux simulated in upward flow module is low relative to that simulated in downward flow module. Then, evapotranspiration spurs matric potential gradient and therefore upward flows are produced. As gravitational potential gradient is always downward, the flow affected by the matric potential gradient is used to simulate upward flows that evapotranspiration spurs, and that's why we refer to this flow as upward flow. Note that the dynamic of unsaturated hydraulic conductivity levels are considered in the downward flow module while neglected (the diffusivity is constant) in the upward flow module over one time-step. In early days following irrigation and precipitation, unsaturated hydraulic conductivity changed rapidly and its dynamic change can be reflected since water flow in this period is mainly simulated from the downward flow module. In later periods, hydraulic conductivity changed so gradually that the dynamic can be neglected in one day. Although not completely accurate, this assumption allowed us to make an approximate estimation.

With low volumes of precipitation and groundwater supplemented to the root zone, upward flows significantly affected crop growth in these areas. To realize the effects of upward flows, the upward flow module was removed from the CSHMUR-EPIC model and the corresponding simulation results were compared with those achieved by the unabridged CSHMUR-EPIC model. As is shown in Fig. 9 and Table 4, the upward flow module improved SWC simulation effects and especially for the upper half of the soil moisture profile. Under a certain amount of deep percolation, actual evapotranspiration and crop yields determined AWP values for arid and semi-arid areas with deep groundwater. Closely related these two components, the SWC for the upper half of the soil profile is a key factor shaping AWP values. Therefore, the upward flow module improving SWC simulations of the upper layers can contribute to the AWP simulation efficiently.

The soil water redistribution module combing downward and upward flows can well simulated SWC values for all soil layers. SWC values of the lower half of the soil profile and that of the upper half of the soil profile were found to be highly correlated with deep percolation and actual evapotranspiration and crop yields, respectively. A conceptual soil hydrological model with this module can be helpful for the simulation of water productivity in arid and semi-arid areas with deep groundwater.

3.3. Simulations in different irrigation scenarios

A qualified model used for management should be capable to simulate the dynamic change of the object. Irrigation schedule in YID was unevenly distributed across space, and average irrigation for corn in 2012 reached 607 mm, accounting for 67% of S2. Seven scenarios involving different irrigation schedules (current conditions (C), average irrigation levels applied the YID (A0), 80% of average irrigation levels (A1), 60% of average irrigation levels (A2), 40% of average irrigation levels (A3), 20% of average irrigation levels (A4) and no irrigation (A5)) were applied for the simulation of S2.

As is shown in Fig. 14, not only over field-capacity deep percolation but also under field-capacity deep percolation not considered in most conceptual soil hydrological models varied with irrigation schedules. The simulated under field-capacity percolation is considerable at

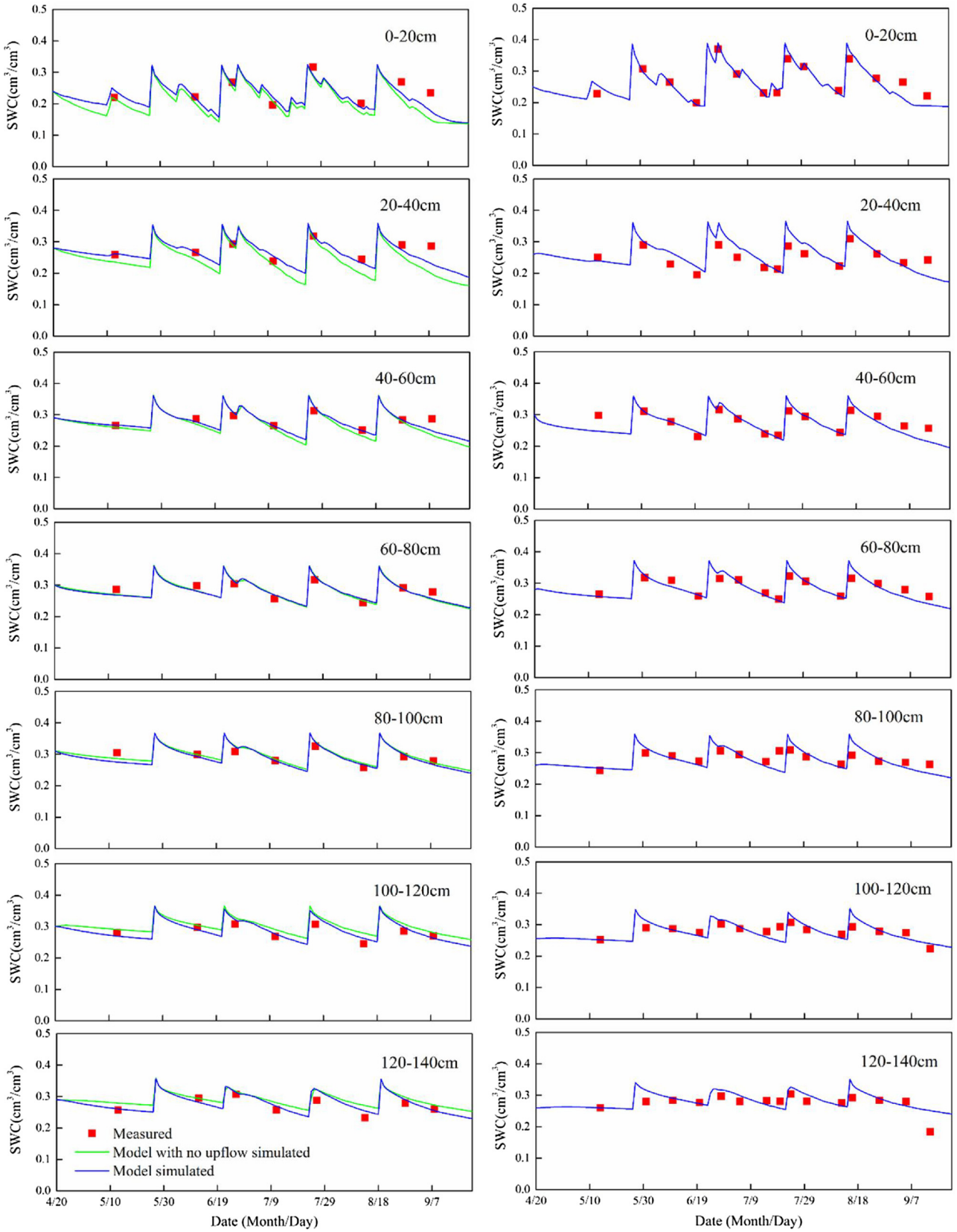

Fig. 9. Simulated versus measured soil water contents in different soil layers during model calibration (left) and validation (right).

normal irrigation conditions and keeps at a low level only if irrigation is too little to arrive at the lowest layer. It ranged from 77 mm to 94 mm in Scenarios C-A1 while from 20 mm to 30 mm in Scenarios A2-A5. Water storage varied in these irrigation scenarios and thus upward flows benefitting crop growth can be dynamically simulated. For these seven irrigation scenarios, relative to simulated Ta values of 222–502 mm, simulated E_a varied little from 79 mm to 129 mm. The caption of the dynamic changes in the productive consumptive use of water (T_a) and

Table 4
Statistical indices on the simulation effect of soil water content in each layer during calibration and validation. Note: the SWC in 0–140 cm soil depth is the average SWC of all the 7 soil layers.

Soil depth	Calibration (with upward flow)				Calibration (no upward flow)				Validation (with upward flow)			
	R^2	RMSE	MRE (%)	NSE	R^2	RMSE	MRE (%)	NSE	R^2	RMSE	MRE (%)	NSE
0–20 cm	0.556	0.029	11	0.436	0.549	0.04	16.8	−0.096	0.903	0.021	6.3	0.815
20–40 cm	0.51	0.022	5.6	0.245	0.539	0.039	13.7	−1.454	0.726	0.033	9.8	−0.09
40–60 cm	0.687	0.015	3.5	0.343	0.686	0.021	6.5	−0.353	0.723	0.023	6.4	0.426
60–80 cm	0.683	0.014	4.8	0.607	0.713	0.014	4.7	0.6	0.843	0.018	4.7	0.524
80–100 cm	0.672	0.014	4.1	0.464	0.748	0.013	3.7	0.588	0.47	0.025	7	−0.836
100–120 cm	0.744	0.015	4.5	0.461	0.795	0.022	6.6	−0.235	0.522	0.021	5.9	−0.086
120–140 cm	0.688	0.017	4.7	0.474	0.721	0.024	7	−0.058	0.362	0.026	7	0.022
0–140 cm	0.793	0.012	3.7	0.692	0.831	0.012	3.8	0.68	0.945	0.014	3.9	0.498

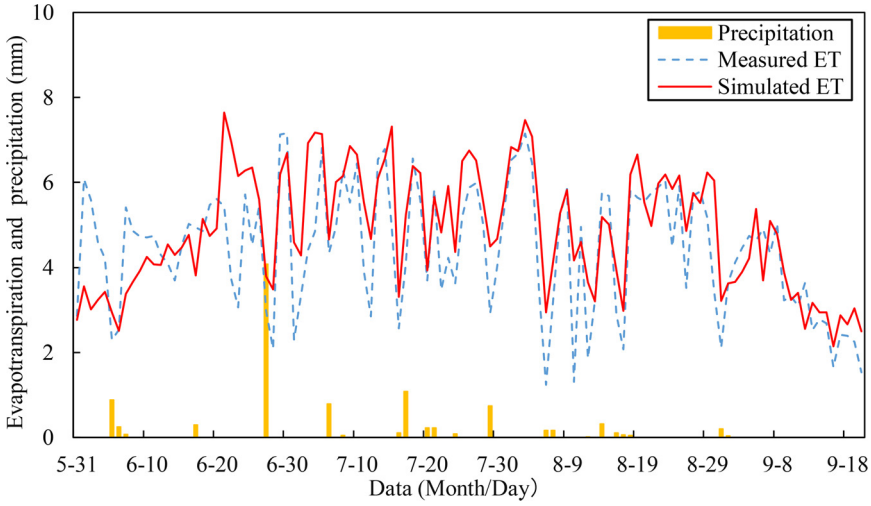

Fig. 10. Comparison of simulated daily evapotranspiration at S2 and measured daily evapotranspiration near S2 with eddy-correlation system.

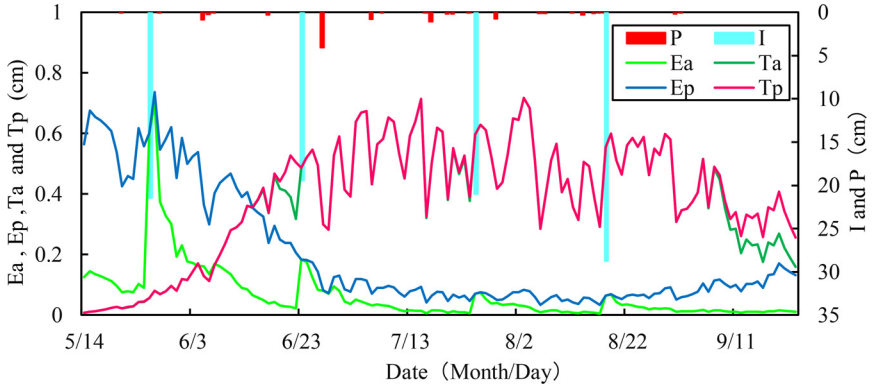

Fig. 11. Model-calculated daily potential and actual evaporation (E_p and E_a), potential and actual transpiration (T_p and T_a), irrigation (I) and precipitation (P) at S2 in 2012.

the non-productive consumptive use of water (E_a) is a key factor for dynamic AWP estimation. Therefore, a model considering the under field-capacity deep percolation is helpful in exploring AWP to obtain a sustainable agricultural water resources management for arid and semi-arid areas with deep groundwater.

4. Conclusions

In this paper, a conceptual soil hydrological model considering under field-capacity redistribution (CSHMUR) was proposed and coupled with the EPIC crop growth model to estimate AWP for rainless area. With field data collected in a typical arid area of northwestern China, the coupled AWP model (CSHMUR-EPIC) was calibrated and validated, and then the effect of the under field-capacity redistribution on the AWP simulation results was investigated. At last, in order to explore the practical application in sustainable agricultural water resources management, the developed AWP model was used as a tool to simulate the dynamic AWP in several irrigation scenarios. Our main conclusions as follows:

1 Drought condition substantially aggravate upward flows produced, and an upward flow module can efficiently improve simulation effects of SWC on the upper half of a soil profile and thus contribute to the estimation of AWP for arid and semi-arid areas.
2 The under field-capacity deep percolation is remarkable and should not be neglected in the AWP estimation for arid areas. According to

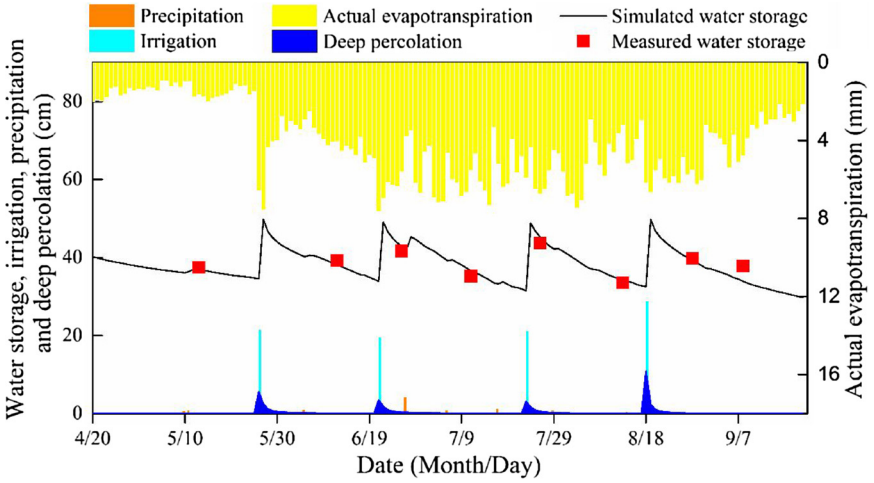

Fig. 12. Simulation results of soil water balance components at S2 in 2012.

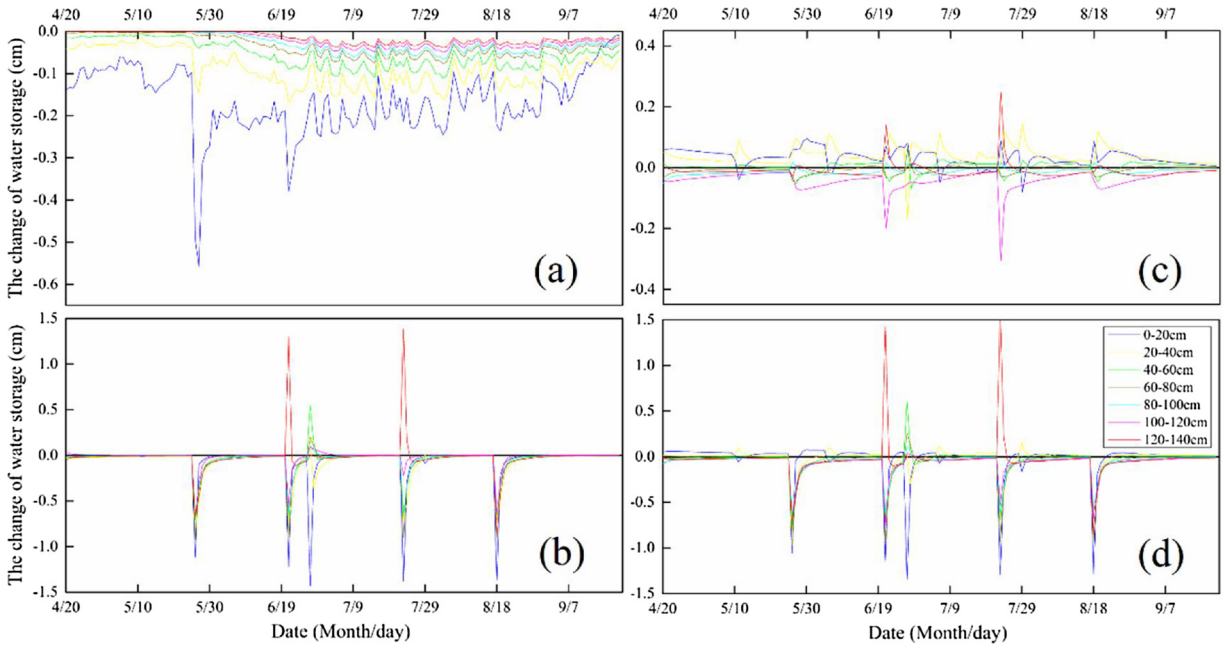

Fig. 13. Simulated water storage changes affected by evapotranspiration (a), gravitational potential gradient (b), matric potential gradient (c) and the resultant of gravitational potential gradient and matric potential gradient (d) at S2 in 2012.

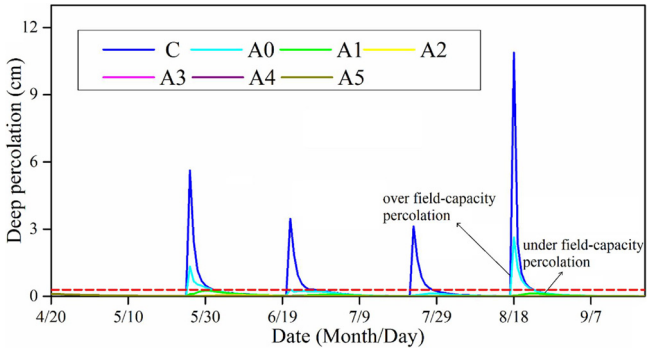

Fig. 14. Simulated deep percolation in different irrigation scenarios at S2 in 2012.

the proposed model, levels reach up to 94 mm with sufficient irrigation, accounting for more than 2/3 of the precipitation measured in our study area. Downward flows embedded in our conceptual soil hydrological model can simulate the under field-capacity deep percolation as well as models based on numerical solutions to the Richards equation.

3 Upward flows and under field-capacity deep percolation not considered in most conceptual soil hydrological models varied with irrigation schedules and thus a hydrological model considering the under field-capacity redistribution has advantages in the exploration of sustainable agricultural water resources management.

Acknowledgments

This study was supported by the National Natural Science Foundation of China (grant numbers: 91425302, 51679236, 51639009). The contributions of the editor and anonymous reviewers whose comments and suggestions significantly improved this article are also appreciated.

References

Allen, R.G., Pereira, L.A., Raes, D., Smith, M., 1998. Crop Evapotranspiration: Guidelines for Computing Crop Water Requirements. FAO Irrigation and Drainage FAO, Rome, pp. 56.

Amarasingha, R.P.R.K., Suriyagoda, L.D.B., Marambe, B., Rathnayake, W.M.U.I., Gaydon, D.S., Galagedara, L.W., Punyawardena, R., Silva, G.L.L.P., Nidumolu, U., Howden, M., 2017. Improving water productivity in moisture-limited rice-based cropping systems through incorporation of maize and mungbean: a modelling approach. Agric. Water Manag. 189, 111–122.

Assouline, S., Russo, D., Silber, A., Or, D., 2015. Balancing water scarcity and quality for sustainable irrigated agriculture. Water Resour. Res. 51 (5), 3419–3436.

Baker, J.M., Griffis, T.J., Ochsner, T.E., 2012. Coupling landscape water storage and supplemental irrigation to increase productivity and improve environmental stewardship in the U.S. Midwest. Water Resour. Res. 48, W05301.

Bellot, J., Chirino, E., 2013. Hydrobal: an eco-hydrological modelling approach for assessing water balances in different vegetation types in semi-arid areas. Ecol. Modell. 266, 30–41.

Belmans, C., Wesselling, J.G., Feddes, R.A., 1983. Simulation model of the water balance of a cropped soil: SWATRE. J. Hydrol. 63 (3–4), 271–286.

Bresler, E., Russo, D., Miller, R.D., 1978. Rapid estimate of unsaturated hydraulic conductivity function. Soil Sci. Soc. Am. J. 42 (1), 170–172.

Chen, S.L., Yang, W., Huo, Z.L., Huang, G.H., 2016. Groundwater simulation for efficient water resources management in Zhangye Oasis, Northwest China. Environ. Earth Sci. 75, 647.

Consoli, S., Papa, R., 2013. Corrected surface energy balance to measure and model the evapotranspiration of irrigated orange orchards in semi-arid Mediterranean conditions. Irrig. Sci. 31 (5), 1159–1171.

Cosgrove, W.J., Loucks, D.P., 2015. Water management: current and future challenges and research directions. Water Resour. Res. 51 (6), 4823–4839.

DeJonge, K.C., Ascough II, J.C., Andales, A.A., Hansen, N.C., Garcia, L.A., Arabi, M., 2012. Improving evapotranspiration simulations in the CERES-maize model under limited irrigation. Agric. Water Manag. 115, 92–103.

Evans, R.G., Sadler, E.J., 2008. Methods and technologies to improve efficiency of water use. Water Resour. Res. 44, W00E04.

Flint, A.L., Flint, L.E., Kwicklis, E.M., Fabryka-Martin, J.T., Bodvarsson, G.S., 2002. Estimating recharge at Yucca mountain, Nevada, USA: comparison of methods. Hydrogeol. J. 10 (1), 180–204.

Gao, X.Y., Huo, Z.L., Qu, Z.Y., Xu, X., Huang, G.H., Steenhuis, T.S., 2017. Modeling contribution of shallow groundwater to evapotranspiration and yield of maize in an arid area. Sci. Rep. 7, 1–13.

Guo, Y., Shen, Y.J., 2016. Agricultural water supply/demand changes under projected future climate change in the arid region of northwestern China. J. Hydrol. 540, 257–273.

Guswa, A.J., 2005. Soil-moisture limits on plant uptake: an upscaled relationship for water-limited ecosystems. Water Resour. Res. 28 (6), 543–552.

Hijmans, R.J., Guiking-Lens, I.M., van Diepen, C.A., 1994. WOFOST 6.0. (User's Guide for the WOFOST 6.0 Crop Growth Simulation Model). Technical Document 12 DLO Winand Staring Centre, Wageningen.

Hillel, D., 1982. Introduction to Soil Physics. Academic Press, San Diego, pp. 364.

Hochmuth, H., Thevs, N., He, P., 2015. Water allocation and water consumption of irrigation agriculture and natural vegetation in the Heihe River watershed, NW China. Environ. Earth Sci. 73 (9), 5269–5279.

Huo, Z.L., Dai, X.Q., Feng, S.Y., Kang, S.Z., Huang, G.H., 2013. Effect of climate change on reference evapotranspiration and aridity index in arid region of China. J. Hydrol. 492, 24–34.

Jiang, Y., Xu, X., Huang, Q.Z., Huo, Z.L., Huang, G.H., 2015. Assessment of irrigation performance and water productivity in irrigated areas of the middle Heihe River basin using a distributed agro-hydrological model. Agric. Water Manag. 147, 67–81.

Jones, C.A., Ritchie, J.T., Kiniry, J.R., Godwin, D.C., 1986. Subroutine structure. Ch. 4 In: Jones, C.A., Kiniry, J.R. (Eds.), CERES-Maize: A Simulation Model of Maize Growth and Development. Texas A&M University Press.

Jones, J.W., Hoogenboom, G., Porter, C.H., Boote, K.J., Batchelor, W.D., Hunt, L.A., Wilkens, P.W., Singh, U., Gijsman, A.J., Ritchie, J.T., 2003. The DSSAT cropping system model. Eur. J. Agron. 18 (3-4), 235–265.

Karandish, F., Simunek, J., 2016. A field-modeling study for assessing temporal variations of soil-water-crop interactions under water-saving irrigation strategies. Agric. Water Manag. 178, 291–303.

Kendy, E., Gerard-Marchant, P., Walter, M.T., Zhang, Y.Q., Liu, C.M., Steenhuis, T.S., 2003. A soil-water-balance approach to quantify groundwater recharge from irrigated cropland in the North China Plain. Hydrol. Process. 17, 2011–2031.

Kendy, E., Zhang, Y.Q., Liu, C.M., Wang, J.X., Steenhuis, T.S., 2004. Groundwater recharge from irrigated cropland in the North China Plain: case study of Luancheng County, Hebei Province, 1949–2000. Hydrol. Process. 18, 2289–2302.

Lee, J.E., Oliveira, R.S., Dawson, T.E., Fung, I., 2005. Root functioning modifies seasonal climate. Proc. Natl. Acad. Sci. U. S. A. 102 (49), 17576–17581.

Li, J., Mao, X.M., Li, M., 2017a. Modeling hydrological processes in oasis of Heihe River Basin by landscape unit-based conceptual models integrated with FEFLOW and GIS. Agric. Water Manag. 179, 338–351.

Li, J., Mao, X.M., Shang, S.H., Steenhuis, T.S., 2017b. Modeling regional soil water balance in farmland of the middle reaches of Heihe River Basin. Water 9 (11).

Li, Y., Kinzelbach, W., Zhou, J., Cheng, G.D., Li, X., 2012. Modelling irrigated maize with a combination of coupled-model simulation and uncertainty analysis, in the northwest of China. Hydrol. Earth Syst. Sci. 16 (5), 1465–1480.

Littleboy, M., Silburn, D.M., Freebairn, D.M., Woodruff, D.R., Hammer, G.L., Leslie, J.K., 1992. Impact of soil erosion on production in cropping systems. I. Development and validation of a simulation model. Aust. J. Soil Res. 30 (5), 757–774.

Liu, J.G., 2009. A GIS-based tool for modelling large-scale crop-water relations. Environ. Model. Softw. 24, 411–422.

Liu, S.M., Xu, Z.W., Song, L.S., Zhao, Q.Y., Ge, Y., Xu, T.R., Ma, Y.F., Zhu, Z.L., Jia, Z.Z., Zhang, F., 2016. Upscaling evapotranspiration measurements from multi-site to the satellite pixel scale over heterogeneous land surfaces. Agric. For. Meteorol. 230–231, 97–113.

López-Cedrón, F.X., Boote, K.J., Pineiro, J., Sau, F., 2008. Improving the CERES-maize model ability to simulate water deficit impact on maize production and yield components. Agron. J. 100 (2), 296–307.

Masikati, P., Manschadi, A., van Rooyen, A., Hargreaves, J., 2014. Maize-mucuna rotation: an alternative technology to improve water productivity in smallholder farming systems. Agric. Syst. 123, 62–70.

McLaughlin, D., Kinzelbach, W., 2015. Food security and sustainable resources management. Water Resour. Res. 51 (7), 4966–4985.

Mendel, M., Hergarten, S., Neugebauer, H.J., 2002. On a better understanding of hydraulic lift: a numerical study. Water Resour. Res. 38 (10), WR000911.

Moriasi, D.N., Arnold, J.G., Van Liew, M.W., Bingner, R.L., Harmel, R.D., Veith, T.L., 2007. Model evaluation guidelines for systematic quantification of accuracy in watershed simulations. Trans. ASABE 50 (3), 885–900.

Morillas, L., Leuning, R., Villagarcia, L., Garcia, M., Serrano-Ortiz, P., Domingo, F., 2013. Improving evapotranspiration estimates in Mediterranean drylands: the role of soil evaporation. Water Resour. Res. 49 (10), 6572–6586.

Nash, J.E., Sutcliffe, J.V., 1970. River flow forecasting through conceptual models part I-A discussion of principles. J. Hydrol. 10 (3), 282–290.

Novark, V., 1987. Estimation of soil-water extraction patterns by roots. Agric. Water Manag. 12 (4), 271–278.

Pereira, L.S., Cordery, I., Iacovides, I., 2012. Improved indicators of water use performance and productivity for sustainable water conservation and saving. Agric. Water Manag. 108, 39–51.

Quijano, J.C., Kumar, P., 2015. Numerical simulations of hydraulic redistribution across climates: the role of the root hydraulic conductivities. Water Resour. Res. 51 (10), 8529–8550.

Raes, D., Steduto, P., Hsiao, T.C., Fereres, E., 2009. AquaCrop-the FAO crop model to simulate yield response to water: II. Main algorithms and software description. Agron. J. 101 (3), 438–447.

Raes, D., Steduto, P., Hsiao, T.C., Fereres, E., 2011. FAO Cropwater Productivity Model to Simulate Yield Response to Water. Reference Manual, Chapter 1 – AquaCrop, Version 3.1Plus.

Richards, J.H., Caldwell, M.M., 1987. Hydraulic lift: substantial nocturnal water transport between soil layers by Artemisia tridentate roots. Oecologia 73 (4), 486–489.

Riha, S.J., Rossiter, D.G., Simoens, P., 1994. GAPS General-Purpose Atmosphere-Plant-Soil Simulator Version 3.0 User's Manual. Department of Soils, Crops and Atmospheric Sciences, Cornell University, Ithaca, NY.

Rijsberman, F.R., 2006. Water scarcity: fact or fiction? Agric. Water Manag. 80 (1–3), 5–22.

Ritchie, J.T., 1972. Model for predicting evaporation from a row crop with incomplete cover. Water Resour. Res. 8 (5), 1204–1213.

Ritchie, J.T., 1996. Soil water balance and plant water stress. Understanding Options/or Agricultural Production. pp. 41–54.

Rose, D.A., 1968. Water movement in porous materials III. Evaporation of water from soil. Br. J. Appl. Phys. Ser. 2 (1), 1779–1791.

Russo, D., Bresler, E., 1980. Scaling soil hydraulic properties of a heterogeneous field soil. Soil Sci. Soc. Am. J. 44 (4), 681–684.

Sau, F., Boote, K.J., Bostick, W.M., Jones, J.W., Minguez, M.I., 2004. Testing and improving evapotranspiration and soil water balance of the DSSAT crop models. Agron. J. 96, 1243–1257.

Sauer, T., Havlik, P., Schneider, U.A., Schmid, E., Kindermann, G., Obersteiner, M., 2010. Agriculture and resource availability in a changing world: the role of irrigation. Water Resour. Res. 46, W06503.

Scanlon, B.R., Healy, R.W., Cook, P.G., 2002. Choosing appropriate techniques for quantifying groundwater recharge. Hydrogeol. J. 10 (1), 18–39.

Scott, R.L., Cable, W.L., Hultine, K.R., 2008. The ecohydrologic significance of hydraulic redistribution in a semiarid savanna. Water Resour. Res. 44 (2), WR006149.

Seyfried, M.S., Schwinning, S., Walvoord, M.A., Pockman, W.T., Newman, B.D., Jackson, R.B., Phillips, E.M., 2005. Ecohydrological control of deep drainage in arid and semiarid regions. Ecology 86 (2), 277–287.

Sharpley, A.N., Williams, J.R., 1990. EPIC-Erosion/Productivity Impact Calculator: 1. Model Documentation. United States Department of Agriculture.

Shi, M.J., Wang, L., Wang, X.J., 2011. A study on changes and driving factors of agricultural water supply and demand in Zhangye after water reallocation of the Heihe River (in Chinese). Resour. Sci. 33 (8), 1489–1497.

Siebert, S., Burke, J., Faures, J.M., Frenken, K., Hoogeveen, J., Doell, P., Portmann, F.T., 2010. Groundwater use for irrigation – a global inventory. Hydrol. Earth Syst. Sci. 14 (10), 1863–1880.

Siska, E.M., Takara, K., 2015. Achieving water security in global change: dealing with associated risk in water investment. Procedia Environ. Sci. 28, 743–749.

Steduto, T., Hsiao, T.C., Raes, D., Fereres, E., 2009. AquaCrop-the FAO – crop model to simulate yield response to water: I. Concepts and underlying principles. Agron. J. 101 (3), 426–437.

Steenhuis, T.S., van der Molen, W.H., 1986. The Thornthwaite–Mather procedure as a simple engineering method to predict recharge. J. Hydrol. 84 (3–4), 221–229.

Stockle, C.O., Martin, S.A., Campbell, G.S., 1994. Cropsyst, a cropping systems simulation-model-water nitrogen budgets and crop yield. Agric. Syst. 46 (3), 335–359.

Suleiman, A.A., Ritchie, J.T., 2003. Modeling soil water redistribution during second-

stage evaporation. Soil Sci. Soc. Am. J. 67 (2), 377–386.
Vaghefi, S.A., Abbaspour, K.C., Faramarzi, M., Srinivasan, R., Arnold, J.G., 2017. Modeling crop water productivity using a coupled SWAT-MODSIM model. Water 9 (3). https://doi.org/10.3390/w9030157.
Wang, J., Huang, G.H., Zhan, H.B., Mohanty, B.P., Zheng, J.H., Huang, Q.Z., Xu, X., 2014. Evaluation of soil water dynamics and crop yield under furrow irrigation with a two-dimensional flow and crop growth coupled model. Agric. Water Manag. 141, 10–22.
Williams, J.R., Jones, C.A., Kiniry, J.R., Spanel, D.A., 1989. The EPIC crop growth model. Trans. ASAE 32, 497–511.
Xu, X., Huang, G.H., Sun, C., Pereirad, L.S., Ramosd, T.B., Huang, Q.Z., Hao, Y.Y., 2013. Assessing the effects of water table depth on water use, soil salinity and wheat yield: searching for a target depth for irrigated areas in the upper Yellow River basin. Agric. Water Manag. 125, 46–60.
Xue, J.Y., Huo, Z.L., Wang, F.X., Kang, S.Z., Huang, G.H., 2018. Untangling the effects of shallow groundwater and deficit irrigation on irrigation water productivity in arid region: new conceptual model. Sci. Total Environ. 619–620, 1170–1182.
Zhao, W.Z., Liu, B., Zhang, Z.H., 2010. Water requirements of maize in the middle Heihe River basin, China. Agric. Water Manag. 97 (2), 215–223.
Zhou, J., Cheng, G.D., Li, X., Hu, B.X., Wang, G.X., 2012. Numerical modeling of wheat irrigation using coupled HYDRUS and WOFOST models. Soil Sci. Soc. Am. J. 76 (2), 648–662.